Lasers in Manufacturing Conference 2019

The impact of different binder systems in laser powder bed fusion of tungsten carbide composites

Tobias Schwanekamp[a*], Gabriela Marginean[b], Martin Reuber[a]

[a]*iWFT Institute of Manufacturing and Tooling Technology, Vogelsanger Str. 295, 50825 Cologne, Germany*
[b]*Westphalian University of Applied Sciences, Neidenburger Str. 43, 45897 Gelsenkirchen, Germany*

Abstract

Laser powder bed fusion (L-PBF) offers significant potentialities for the design of innovative cutting tools. Industrial applications are hitherto limited to steel alloys since laser molten carbides such as WC-Co exhibit defects like pores, cracks, eta-phases, evaporation of binder and excessive WC-grain growth. Previous research indicates that thermal cracking can be prevented by high-temperature pre-heating. However, WC-grain growth and residual η-phases remain and need countermeasures. For conventional sintering, it is well known that the formation of phases depends on the carbide-binder system and chromium-based additives are used as WC grain growth inhibitors. Therefore, a fundamental study on nickel and cobalt-chromium as alternative binder systems in L-PBF of tungsten carbides is conducted. The results are compared to those of the WC-Co system. Samples from WC-CoCr and WC-Ni powders are generated at 800°C pre-heating temperature. Analysis is undertaken with respect to mechanical properties and material defects. Furthermore, microstructure, binder evaporation, WC-grains and phase development are analyzed.

Keywords: laser powder bed fusion, L-PBF, SLM, tungsten carbide, binder, additive manufacturing, cutting tools

1. Introduction and Theory

Industrial applications of Laser Powder Bed Fusion (L-PBF) in cutting tool manufacturing are still limited to the processing of a few steel alloys. A sufficient quality for carbide materials, such as WC-Co, is not yet achieved. An overview of the research on L-PBF of WC-Co, conducted from 2010 to 2015 by different institutions, was published by Uhlmann et al. 2015. A conflict between the reduction of residual pores and the

* Corresponding author. Tel.: +49-221 54687-743; fax: +49-221 54687-36.
E-mail address: tobias.schwanekamp@rfh-koeln.de.

prevention of cobalt evaporation during the L-PBF process was pointed out. High laser energy inputs cause an increased amount of liquid phase inside the melting pool, which leads to an improved wetting behavior and a reduction of porosity. On the other hand, high energy inputs cause embrittlement due to a significant evaporation of cobalt binder and, in combination with the high temperature gradients, the formation of thermal cracks. Decarburization of the WC phase was also detected, which leads to further embrittlement due to the formation of W_2C- and η-carbides. The conflict mentioned by Uhlmann was also confirmed by Schwanekamp and Reuber 2016 and cannot solely be solved by an optimization of the main L-PBF parameters such as laser power P, scan speed v, hatch distance h and layer thickness Δs. A significant improvement of the material quality was achieved by high temperature pre-heating above 800°C, published by Schwanekamp and Reuber 2018. Thermal cracking can be fully prevented and porosity can substantially be reduced within a wide L-PBF parameter range. However, the material is still characterized by a heterogeneous microstructure, Co-agglomerations and WC-grain growth as well as binder evaporation, residual pores and η-phases, resulting in inferior mechanical properties compared to conventional WC-Co material (Figure 1).

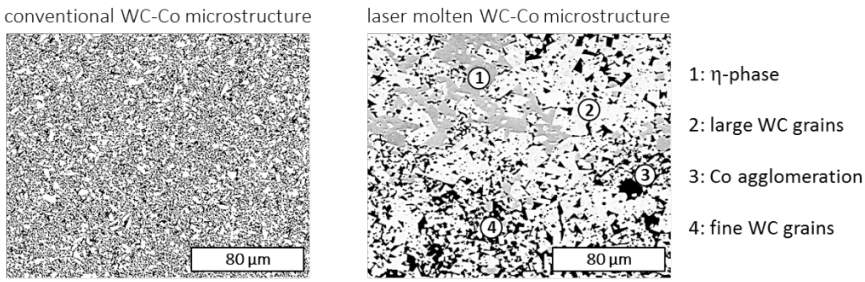

Fig. 1. Comparison of conventionally sintered and laser molten WC-Co microstructure (SEM-BSE images)

From conventional sintering it is known that the formation of phases within carbide binder systems strongly depends on the binder material used. A partial or total substitution of the traditional cobalt binder, in particular by more economic or less toxic materials such as nickel and iron, has been subject of research activities on sintering processes for many years. One of the first fundamental descriptions of phases in the Co-W-C, Ni-W-C and Fe-W-C systems was already published by Takeda 1936. Guillermet 1989 presented a thermodynamic description of the Co-Fe-Ni-W-C system to gain insight into the effects of substitution of Co by Fe and Ni. An extensive review on W-C phase diagrams with different binders such as Co, Fe, Ni, Al and Cr is given by Fernandes and Senos 2011. Furthermore, a lot of research is published on thermally sprayed WC-CoCr, e.g. by Suhonen et al. 2009 and Kazamer et al. 2016. However, there is no literature about L-PBF of WC with alternative binder systems, yet. Therefore, a preliminary study on L-PBF of WC-Ni and WC-CoCr is conducted and presented in this paper. Specimens made by L-PBF are analyzed with respect to the microstructure, the phase and elemental balance, WC-grain growth and the mechanical properties of the laser molten material, depending on the L-PBF process parameters.

2. Materials and Methods

2.1. Generation and analysis of specimens

All experiments are conducted on a Renishaw AM 250 system under inert gas atmosphere (nitrogen 5.0) at an elevated base plate temperature of 800°C. A standard meander scan pattern is applied using a 200 W fiber laser with a focal diameter of d_f = 75 µm (Gaussian mode, TEM_{00}). Simple cubic specimens are generated under variation of laser power from P_{min} = 36 W to P_{max} = 200 W, scan velocity from v_{min} = 36 mm/s to v_{max} = 200 mm/s and hatch distance from h_{min} = 36 µm to h_{max} = 200 µm. The layer thickness is kept on a

constant value of $\Delta s = 30$ µm. All specimens are built on WC-Co (90/10) substrate. To reduce the experimental effort, a central composite design of experiments (DoE) consisting of 15 different parameter settings is implemented for the generation of samples. Based on the measurements on the samples the correlation between the input parameters P, v and h and the responses (e.g. porosity and hardness) can be approximated by second order regression models. The same approach was already applied for the studies on WC-Co 88/12 and 83/17, published by Schwanekamp and Reuber 2018. The impact of variations in laser power P, scan velocity v and hatch distance h on properties and microstructure of the laser molten material is evaluated applying methods described in the following. The occurrence of thermal cracking and pores inside the material is detected by microscopic analysis of polished cross sections. The proportion of elements, phase composition and material microstructure inside the specimens are analyzed by scanning electron microscopy (SEM), energy dispersive X-ray spectroscopy (EDX) and X-ray diffraction (XRD). Due to the experimental effort, the XRD analyses are only conducted for a selection of specimens. The Vickers hardness of the samples is measured according to ISO 3878 with a test load of 29,42 N (HV3). Besides the Vickers hardness, the transverse rupture strength (T.R.S.) is of importance for potential cutting tool applications. For this purpose, samples are generated via L-PBF, ground to size and tested in a three-point bending test according to ISO 3327:2009.

2.2. Powder material

For the present study, agglomerated and pre-sintered WC-Ni and WC-CoCr thermal spray powders are used. Table 1 gives an overview of the nominal powder specifications as provided by the factory certification report from DURUM VERSCHLEISS-SCHUTZ GMBH. SEM images of the powders are shown in Figure 2. The particles are compact and the grain size distributions are appropriate for the L-PBF process. The WC-Ni grains are larger and more spherical in comparison to the WC-CoCr grains. However, a sufficient flow capability for the L-PBF process is achieved with both powders. XRD analysis of the WC-Ni powder only indicated WC and Ni phases. For the WC-CoCr a small amount of W_2C phase is detected in addition to the WC and CoCr phase. Some of the results are also compared with the WC-Co system. The WC-Co specimens were generated in the framework of a former publication, where detailed information about the WC-Co powders can be found (Schwanekamp and Reuber 2018).

powder type (DURMAT)	**103.007**	**115.021**
powder type	WC-Ni (88/12)	WC-CoCr (86/10/4)
chemical composition (manufacturer report)	Ni: 12 ± 1 wt-% WC: res.	Co: 10 ± 1 wt-% Cr: 4 ± 0.5 wt-% WC: res.
particle size	-45 + 15 µm	-30 + 10 µm
WC-grain size	2.5 µm	1.3 µm

Table 1. Material data of the processed powder types provided by DURUM VERSCHLEISS-SCHUTZ GMBH

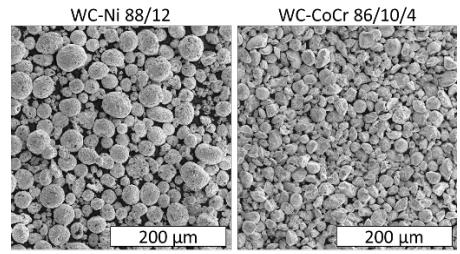

Fig. 2. SEM images of the thermal spray powders used for the current study

3. Experimental Results and Discussion

3.1. WC-Ni

The experimental results are based on the parameter variations from the central composite DoE. They are shown in comparison to results gained in a previous study, when WC-Co (88/12) was analyzed under the same experimental setup and parameter set (Schwanekamp and Reuber 2018). Figure 3 shows the polished

cross-sections of specimens generated from WC-Co (88/12) and WC-Ni (88/12) powder with three different laser power settings. The same trend of the porosity ϕ can be observed for both material systems. For very low laser power, large irregular pores are formed by insufficient wetting of the liquid phase during the L-PBF process. Minimum porosity is achieved for medium laser power. For very high laser power, a slight increase in ϕ can be observed as a result of evaporation effects. Quantitative and qualitative analysis of the samples shown in Figure 3 indicates that the porosity is lower for WC-Ni, in particular for low laser power. For confirmation, a second order response surface model is established based on the results of the design of experiments within the entire parameter field. Figure 4 shows the resulting contour plots of the porosity depending on the laser power P, the scan velocity v and the hatch distance h. As a result, the lower porosity can be confirmed for the WC-Ni material system compared to WC-Co in a wide range of parameter variations.

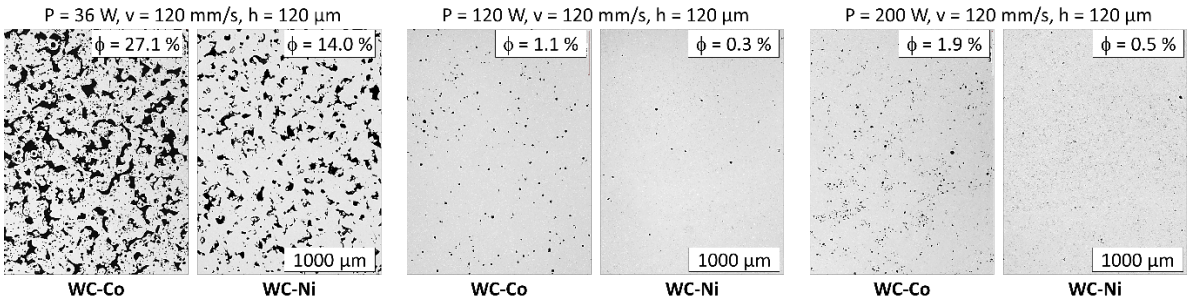

Fig. 3. Polished cross-sections of specimens generated from WC-Co 88/12 and WC-Ni 88/12 with three different values of laser power P under constant scan velocity (120 mm/s) and constant hatch (120 µm)

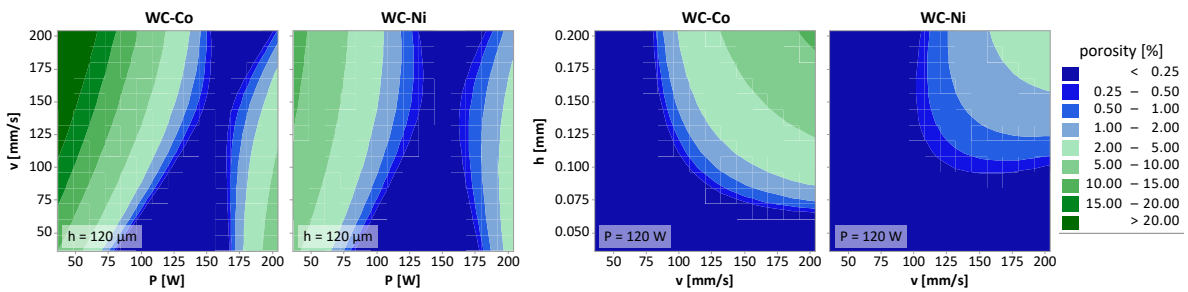

Fig. 4. Contour plots of the established second order response surface models for porosity ϕ; comparison of WC-Co and WC-Ni samples under large variation of P, v and h.

The amount of residual binder in comparison to the initial powder material is measured by means of EDX analysis. Similar trends and magnitudes in binder evaporation with variation of P, v and h are observed for WC-Co and WC-Ni in the main effects plots in Figure 5 a). Parameter settings which lead to an increase in the specific energy input E_V cause a significant decrease in the residual binder content. For WC-Ni the effect of binder evaporation is even more evident, which is consistent with research in conventional sintering and can be explained by the higher vapor pressure of nickel in comparison to cobalt (Fernandes and Senos 2011). It must be noted that the susceptibility to crack formation increases with decreasing residual binder content. If the residual binder content is lower than 2.5 wt.-%, cracks could not be prevented for any of the specimens, for WC-Co as well as for WC-Ni, as shown in Figure 5 b). Full absence of cracks was achieved for all tested samples with a residual binder content above 3.5 wt.-% (WC-Co), respectively 6.5 wt.-% (WC-Ni). For residual binder contents between those values, cracks occurred sporadically in some of the samples with decreasing trend towards higher binder contents. These results indicate, that the WC-Ni system appears to be more prone to the formation of cracks than the WC-Co system.

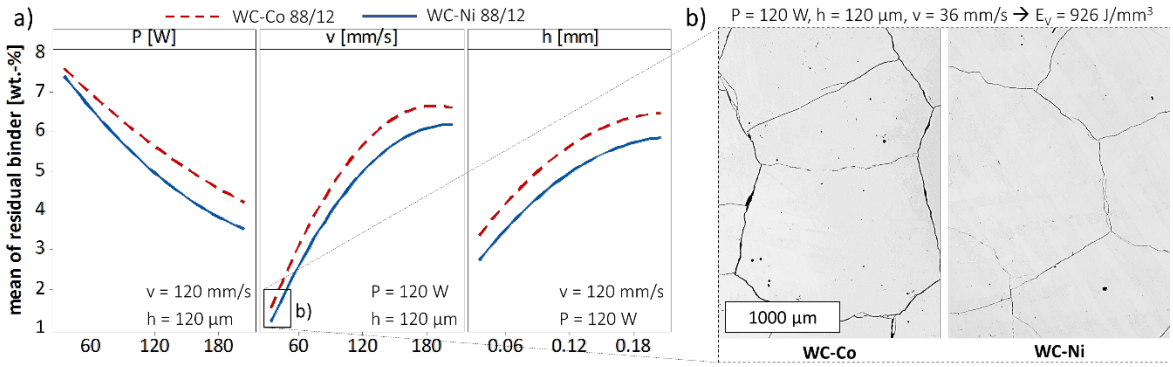

Fig. 5. Main effects plots for the mean of residual binder content (a) and polished cross-sections of cracked specimens with low amount of residual binder (b)

The amount of binder is significantly affecting the Vickers hardness of cemented carbides (Spriggs 2002). With increasing binder ratio the content of hard particles and thereby the hardness is decreasing. Consequently, a clear inverse correlation between binder evaporation and Vickers hardness is observed. Figure 6 a) shows the impact of P, v and h on the mean of Vickers hardness of the generated samples in a main effects plot. The trends are similar for WC-Co and WC-Ni and inverse to the amount of residual Co, respectively Ni, shown in Figure 5 a). Increasing laser energy inputs E_V, caused by increased P or decreased v and h, lead to higher binder evaporation by trend, consequently to an increased Vickers hardness. Additionally a decomposition of the WC grain structure can be seen as shown in Figure 6 b) and Figure 6 c). These figures compare the microstructure close to a Vickers indent for a high and a moderate specific energy input.

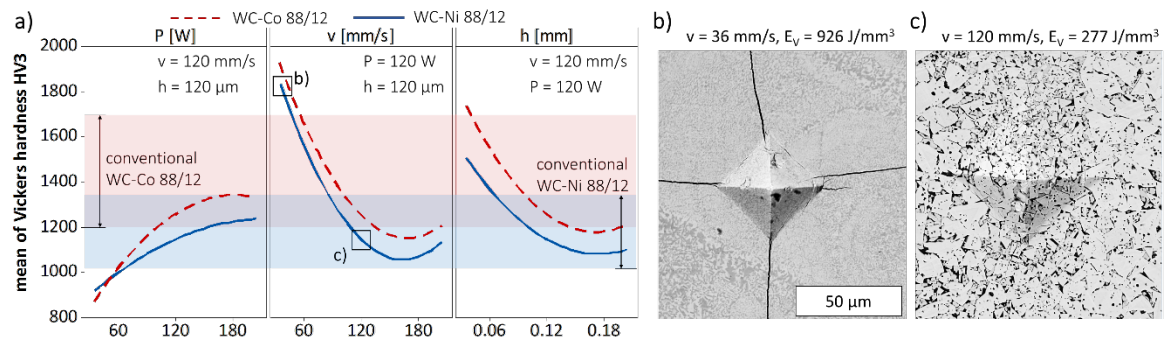

Fig. 6. Main effects plots for the mean of Vickers hardness HV3 (a), Vickers indents for a sample with low residual Ni content and high Vickers hardness (b) and with higher residual Ni content and lower Vickers hardness (c)

In Figure 6 b, a microstructure generated with E_V = 926 J/mm^3 shows that the typical WC grain structure is no longer apparent. The extensive embrittlement causes a decrease in the fracture toughness and characteristic cracks emanating from the edges of the Vickers indent. The same observation is well-known in the measurement of fracture toughness for Co-binder systems (Spiegler et al. 1990). In samples generated with moderate energy inputs (E_V = 277 J/mm³), as shown in Figure 6 c), the WC grain structure is still present and interspersed with binder, even though the WC grains are significantly grown and a certain amount of undesired phases is observed between the grains. Still, the hardness of additively manufactured materials is reduced in comparison to the conventionally sintered material. This can be attributed to WC grain growth, which reduces both, hardness and toughness (Spriggs 2002). Furthermore, volumetric defects such as pores can cause a significant degradation of the material resistance against the Vickers indent (Morrell 1990). Gen-

erally, the hardness is lower for WC-Ni than for WC-Co, which is in agreement to the expectations and the same for conventionally sintered material.

Besides the Vickers hardness, the transverse rupture strength (T.R.S.) is another important quality feature, especially for cutting tool applications. The T.R.S. of composite carbides mainly depends on the binder content and the carbide grain size. For laser molten carbides, the T.R.S. is also affected by characteristic defects such as pores and cracks. In this study, at least three samples of each parameter setting are generated to consider process related variances. The maxima of T.R.S. and the trends which are found for the dependency of the T.R.S. from the main process parameters P, v and h are shown in Figure 7 a). The trends are basically similar to those shown for the WC-Co system by Schwanekamp and Reuber 2018. Maxima in T.R.S. are found for combinations of high P-, v-, h-values, leading to a rather low E_V-value of 196 J/mm^3 as well as for combinations of low P-, v-, h-values with a medium E_V of 476 J/mm^3.Those samples showed exceptionally high T.R.S. values of 1680 MPa for the medium energy input, respectively 1520 MPa for low energy in the building process.

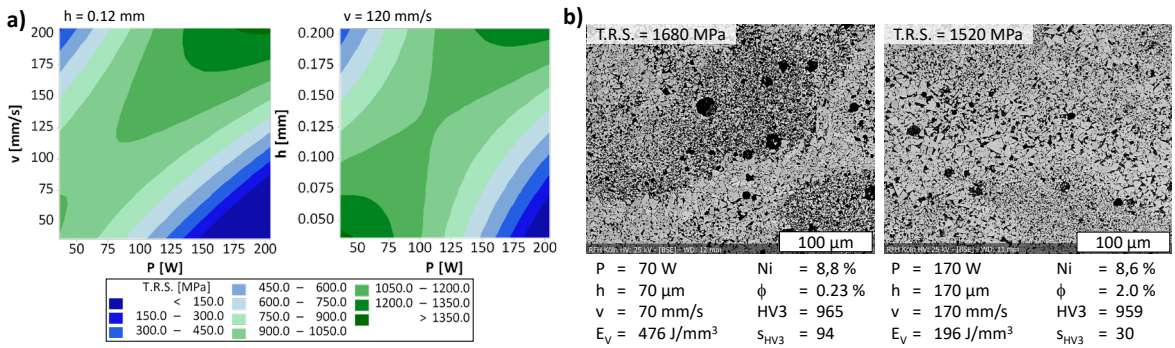

Fig. 7. Contour plots for the mean of T.R.S. (a), SEM (BSE) micrograph of two selected samples with high T.R.S. (b)

Visual microstructural analysis (SEM/BSE) of the two samples revealed large regions with small WC grains embedded in the Ni matrix, Figure 7 b). Due to the low to medium energy input, binder evaporation stays small and a high amount of residual Ni is detected. Both effects lead to an increase the T.R.S. However, in comparison to conventional WC-Ni, the T.R.S. of these samples is still 35-50% lower. This can be expected due to partial WC grain growth, residual porosity, binder evaporation and heterogeneity in the microstructures, generally observed in additively manufactured carbide systems and already described by Schubert et al. 2017; Schwanekamp and Reuber 2016, 2018; Uhlmann et al. 2015. From those previous investigations on WC-Co it is also known that the decomposition of carbides and the formation of W_2C and η-phases drastically increases with the induced laser energy E_V. In this study, XRD analysis is applied for identification of phase composition in the laser molten WC-Ni samples. Due to the experimental effort, XRD is only conducted for a selection of samples with low to moderate energy input and T.R.S. values above 1000 MPa. The results show that W_2C and η-phases are detected in all these samples. Therefore, it can be assumed with high certainty, that the samples generated with higher energy input also contain η-phases. Figure 8 shows the comparison of an XRD pattern for the initial powder and for a sample generated with the same parameter setting already shown in Figure 7 b) (right). Besides the original WC and Ni phases in the powder material, small amounts of additional W_2C and Ni_2W_4C η-carbides are detected by XRD and also visualized in an SEM/BSE micrograph by the light grey phases between the WC grains (encircled in Figure 8). For slightly higher energy inputs (E_V = 278 J/mm^3), traces of graphite phase are also detected.

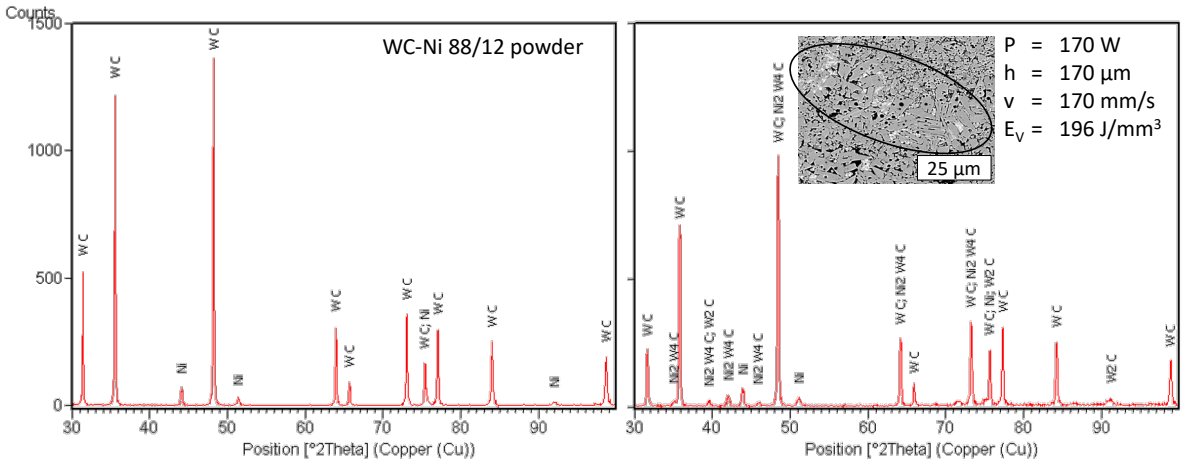

Fig. 8. XRD patterns of the initial WC-Ni 88/12 powder (left) and a WC-Ni sample generated by L-PBF with low E_V (right)

3.2. WC-CoCr

The samples generated from WC-CoCr (86/10/4) powder are built with the same DoE parameter settings being applied for the WC-Ni-System. Due to the small amount of WC-CoCr powder available in this study, a generation of adequate samples for bending tests and a reliable evaluation of T.R.S. was not possible. An analysis of the porosity within the DoE parameter range indicated similar trends already shown for WC-Co and WC-Ni in Figure 4. However, the resulting contour plots of the porosity given in Figure 9 a) indicate, that the porosity of the WC-CoCr material system is slightly higher compared to WC-Co in the considered range of parameter variations. This can also be seen by direct comparison of polished cross sections between WC-Co and WC-CoCr in Figure 9 b).

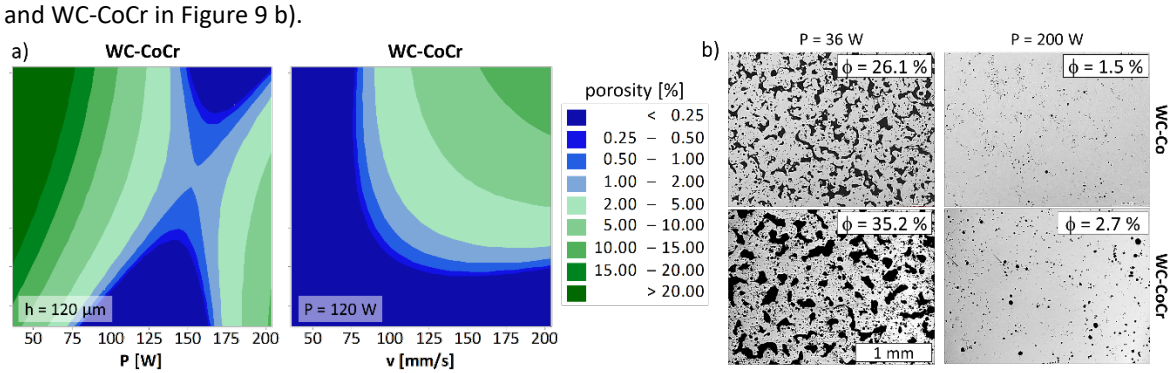

Fig. 9. Contour plots of the established second order response surface models for porosity ϕ of WC-CoCr under wide variation of P, v and h (a); comparison of WC-Co and WC-CoCr samples under variation of P (v = 120 mm/s, h = 120 µm) (b)

The evaporation of binder is analyzed and shown in the main effects plot in Figure 10 a). As seen for WC-Co and WC-Ni, the evaporation and thereby the Vickers hardness (Figure 10 b)) increases for parameter settings leading to increase in energy input. For WC-CoCr it can be noted, that all specimens with residual binder contents above 3 wt.-% were completely free of cracks. In total, the residual binder content (Co+Cr) is higher compared to the other materials shown in Figure 5, which can easily be explained by the higher initial binder content of 14% in comparison to 12% for WC-Co and WC-Ni. Nevertheless, the measured Vickers

hardness is slightly higher and less affected by P, v and h for WC-CoCr in a wide parameter field as shown in Figure 10 b).

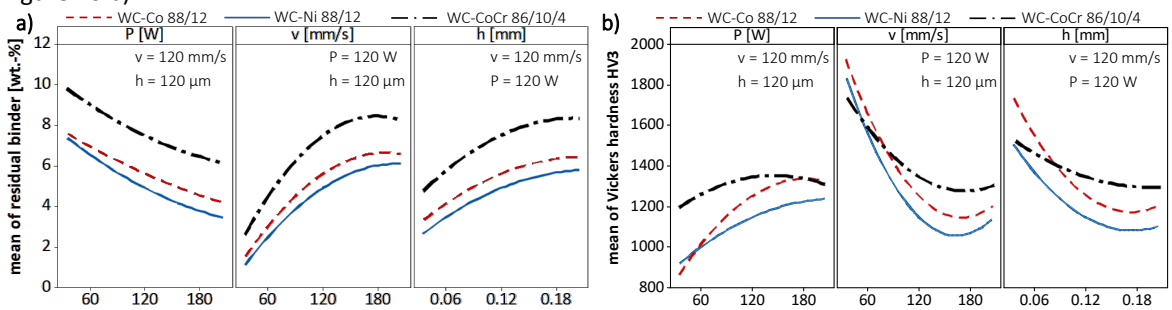

Fig. 10. Comparison of WC-Co, WC-Ni and WC-CoCr in main effects plots; main effects plots for the mean of residual binder content (a); main effects plots for the mean of Vickers hardness HV3 (b).

A potential explanation can be found looking into the microstructure of the WC-CoCr samples. Figure 11 shows an SEM-BSE micrograph and an EDX mapping of a sample, generated with medium laser power, scan velocity and hatch distance. Chromium is detected inside the carbide grains to some extent. Furthermore, even for this moderate energy input, a high amount of tungsten (W) is detected in the binder phase outside the WC grains, which is an indicator for η-phase formation, leading to embrittlement and increase of hardness. This visual analysis of η-phase formation is also confirmed by the XRD patterns shown in Figure 12, indicating that CoCr binder phase and W_2C cannot be detected any more in the laser molten material. Instead, a high amount of η-carbides (Co_3W_3C) as well as traces of chromium carbide ($Cr_{23}C_6$) are detected. Slight variations in the main process parameters and further reduction of E_V did not significantly affect the phase composition as shown by comparison of the two XRD patterns in Figure 12.

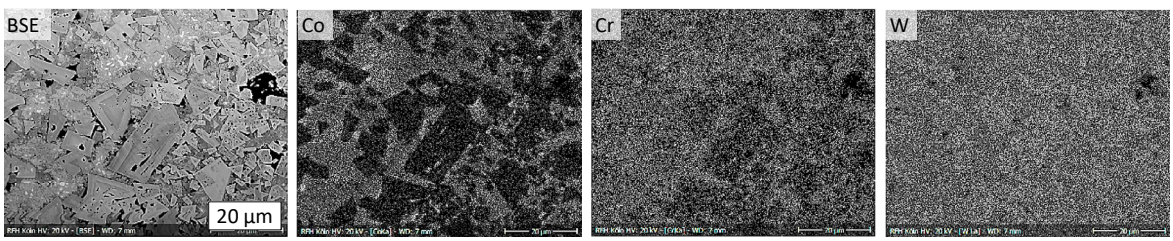

Fig. 11. BSE image and EDX mapping of a sample generated from WC-CoCr (P = 120 W, v = 120 mm/s, h = 120 µm)

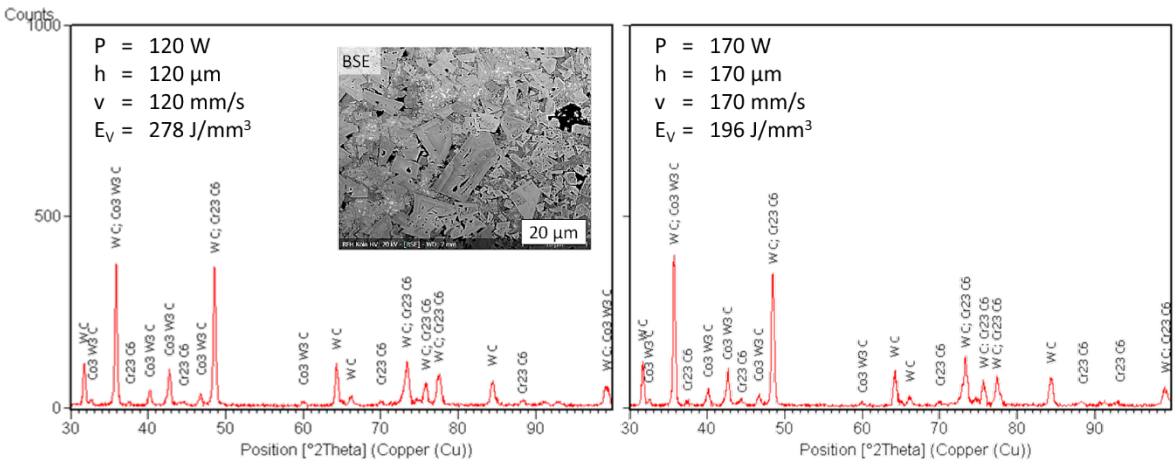

Fig. 12. XRD patterns of WC-CoCr samples generated by L-PBF with moderate E_V (left) and low E_V (right)

Chromium carbide is used as grain growth inhibitor for conventional sintering. Hence, an effect of Cr on the grain growth for the L-PBF generated WC-CoCr system might also be expected, in particular, since the EDX mapping indicated an inclusion of chromium into the carbide grains. The measurement equipment within this study does not allow for a quantitative comparison between grain size distributions of the investigated material systems. However, Figure 13 shows a direct comparison of SEM (BSE) micrographs for different WC material systems, processed by L-PBF under the same conditions and parameters. Visual evaluation indicates a heterogeneous distribution of grain sizes for all samples. However, the largest grain sizes are observed for WC-Co 83/17 powder whereas the smallest grains sizes with a good embedding of the grains in the matrix are observed for the WC-Ni samples, which also exhibited the highest T.R.S. values. A significant effect of chromium on the inhibition of grain growth is not detected. However, the visual identification of grain boundaries is most difficult for the WC-CoCr samples, due to the low contrast between carbide grains and matrix. This is caused by high saturation of tungsten inside the matrix and large regions which are not fully crystallized (encircled area).

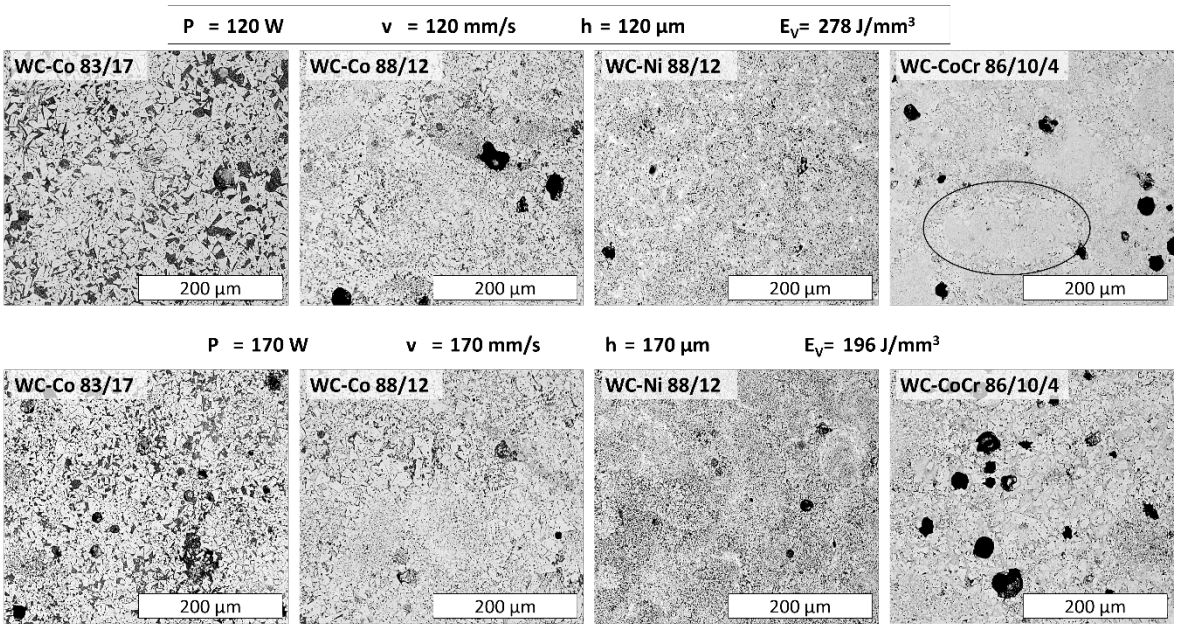

Fig. 13. SEM (BSE) images of microstructures generated from different powder materials and L-PBF settings

4. Summary and Outlook

A preliminary study on L-PBF of WC-Ni and WC-CoCr is conducted and presented in this paper. Samples are generated by L-PBF under variation of the main process parameters at 800°C pre-heating temperature and analyzed with respect to porosity, microstructure, phase and elemental balance, WC-grain growth and mechanical properties such as Vickers hardness and transverse rupture strength (T.R.S.). The findings of the study are evaluated against the results on L-PBF of WC-Co. The fundamental trends and dependencies of porosity, binder evaporation, embrittlement and hardness on laser power P, scan velocity v and hatch distance h are already published for WC-Co and are very similar for WC-Ni and WC-CoCr. However, the following specific findings can be summarized from this study:

- In comparison to WC-Co 88/12, the overall porosity in the samples generated by L-PBF is lower for WC-Ni and slightly higher for WC-CoCr within the investigated parameter field.
- The evaporation of binder significantly affects the formation of cracks. For WC-CoCr cracks were fully prevented with residual binder contents higher than 3 wt.-%. For WC-Ni, higher residual binder contents (> 6.5% wt.-%) are required for full prevention of cracks. In comparison, crack free samples from WC-Co 88/12 are achieved with residual binder contents higher than 3.5 wt.-%.
- η-carbides are detected by XRD in all investigated laser molten WC-Ni and WC-CoCr samples, even for low laser energy inputs. In particular, for the WC-CoCr system is observed that almost the full binder matrix is transformed into η-carbides.
- A significant impact of chromium on WC grain growth is not detected. The smallest grain sizes are observed for the WC-Ni system. Even if residual pores are present, these samples indicated the highest T.R.S. values published up to now for L-PBF of cemented carbides, indicating that the grain size is one of the key impact factors.

Further work will therefore put an emphasis on detailed investigation of impact factors on the WC grain sizes of WC-Co and WC-Ni systems during L-PBF.

Acknowledgements

Parts of the presented work are conducted in the framework of the project “PraeziGen” and supported by the Federal Ministry of Education and Research (BMBF) under the topic of “Photonische Prozessketten”, support code: 03XP0012H. The authors gratefully acknowledge the contribution of the associated project partners. Furthermore, a great debt of gratitude is owed to Andreas Müller, Guillermo Lería Morillo and Daniel Poddig, student researchers at the iWFT, for their significant contribution to the materials testing.

References

Fernandes, C. M. and A. M. R. Senos 2011. ‘Cemented carbide phase diagrams: A review’, *International Journal of Refractory Metals and Hard Materials*, 29/4 (2011), 405–418.

Guillermet, A. F. 1989. ‘The Co-Fe-Ni-W-C Phase Diagram: A Thermodynamic Description and Calculated Sections for (Co-Fe-Ni)-Bonded Cemented WC Tools’, *Zeitschrift für Metallkunde*, 80(2) (1989), 83–94.

Kazamer, N., D. T. Pascal, G. Marginean, V.-A. Serban, W. Brandl, and P. C. Valean 2016. ‘Aspects concerning the wear and corrosion behaviour of WC-CoCr coatings and respectively DLC/WC-CoCr systems’, in *Conference proceedings of NANOCON 2016* presented at the *NANOCON 2016* (Brno, Czech Republic: 2016), 383–389.

Morrell, R. 1990. *Guidelines for Conducting Hardness Tests on Advanced Ceramic Materials*, VAMAS Report 8 (ISSN 1016 - 2186) (Teddington, Middlesex, UK: National Physical Laboratory, 1990).

Schubert, T., A. Breninek, T. Bernthaler, D. Sellmer, M. Schneider, and G. Schneider 2017. ‘Investigations on Additive Manufacturing of WCCo Hard Metals by Laser Beam Melting’, *Practical Metallography*, 54/9 (2017), 577–595.

Schwanekamp, T. and M. Reuber 2016. ‘Additive Manufacturing of application optimized tungsten carbide precision tools’, in *Proceedings of 6th International Conference on Additive Technologies* presented at the *6th International Conference on Additive Technologies - iCAT 2016* (Nürnberg, Germany: Interesansa - zavod, Ljubljana, 2016), 100–114.

Schwanekamp, T. and M. Reuber 2018. ‘Parameter study on laser beam melting of WC-Co at 800°C pre-heating temperature’, in *Proceedings of 7th International Conference on Additive Technologies* presented at the *7th International Conference on Additive Technologies - iCAT 2018* (Maribor, Slovenia: Interesansa - zavod, Ljubljana, 2018), 78–84.

Spiegler, R., S. Schmauder, and L. S. Sigl 1990. ‘Fracture toughness evaluation of WC-Co alloys by indentation testing’, *J. Hard Mater*, 1/3 (1990), 147–158.

Spriggs, G. E. 2002. ‘13.4 Properties of hardmetals and cermets’, in *Powder Metallurgy Data. Refractory, Hard and Intermetallic Materials*, Landolt-Börnstein (Springer, 2002), 86–117.

Suhonen, T., T. Varis, E. Turunen, X. Liu, Y. Ge, O. Söderberg, and S.-P. Hannula 2009. ‘The effect of microstructure on mechanical properties of HVOF sprayed WC-CoCr composite coatings’, *Tribologia - Finnish Journal of Tribology*, 28/1–2 (2009).

Takeda, S. 1936. ‘A Metallographic Study of the Action of the Cementing Materials for Cemented Tungsten Carbide’, *Tohoku Imperial University - Science Reports*, Anniversary Volume, Sendai (1936), 18.

Uhlmann, E., A. Bergmann, and W. Gridin 2015. ‘Investigation on Additive Manufacturing of Tungsten Carbide-cobalt by Selective Laser Melting’, *Procedia CIRP*, 35 (2015), 8–15.